PNAS
www.pnas.org

Supplementary Information for

Feedforward information and zero-lag synchronization in the sensory thalamo-cortical circuit are modulated during stimulus perception

Adrià Tauste Campo, Yuriria Vázquez, Manuel Álvarez, Antonio Zainos, Román Rossi-Pool, Gustavo Deco, and Ranulfo Romo

Email: rromo@ifc.unam.mx, adria.tauste@gmail.com

This PDF file includes:

Supplementary text
Figs. S1 to S7
References for SI reference citations

www.pnas.org/cgi/doi/10.1073/pnas.1819095116

Supplementary Information Text

Methods

Detection task

Stimuli were delivered to the skin of the distal segment of one digit of the restrained hand, via a computer-controlled stimulator (BME Systems, MD; 2-mm round tip). The initial probe indentation was 500 μm. Vibrotactile stimuli consisted of trains of 20 Hz mechanical sinusoids (20 ms duration each sinusoid), with amplitudes of 1-34 μm (Fig. 1A). These were interleaved with an equal number of trials where no mechanical vibrations were delivered to the skin (amplitude = 0). A trial began when the probe tip (PD) indented the skin of one fingertip of the restrained, right hand, upon which the monkey placed its free, left hand on an immovable key (KD). After a variable pre-stimulus period (1.5-3 s), a vibrotactile stimulus could be presented or not (0.5 s). After a fixed delay period (3 s), the stimulator probe was lifted off from the skin (PU), indicating to the monkey that it could initiate the response movement (KU) to one of two buttons (PB). The button pressed indicated whether or not the monkey felt the stimulus (henceforth referred as 'yes' and 'no' responses, respectively). They were rewarded with a drop of liquid for correct responses. Psychometric detection curves were obtained by plotting the proportion of 'yes' responses as a function of the stimulus amplitude (left panel of Fig. 1B). Depending on whether the stimulus was present or absent and on the behavioral response, the trial outcome was classified as hit, miss, false alarm or correct rejection (right pane of Fig. IB). Monkeys were handled according to the institutional standards of the National Institutes of Health and Society for Neuroscience. All protocols were approved by the Institutional Animal Care and Use Committee of the Instituto de Fisiología Celular of the National Autonomous University of Mexico (UNAM).

In addition to the experimental condition described above, the animals also performed a passive control task (referred as passive condition) during which the stimulus was present or absent, but no response was required (1). Monkeys were

rewarded randomly during the occurrence of the passive condition. Under this situation, sensory information enters or not to the somatosensory system, but no decision and perceptual report is required to obtain a reward.

Recordings

Neuronal recordings were obtained by using two arrays, each with seven independent, movable microelectrodes (2 −3 MΩ; [2, 3]). One array was inserted into S1 (cyan spot on the figurine of left panel of Fig. 1C), in the cutaneous representation of the fingers (areas 1 or 3b; middle panel of Fig. 1C). The other array was located lateral and posterior to the hand's representation (green spot on the figurine of left panel of Fig. 1C) in a way that allowed us to lower the microelectrodes to the cutaneous representation of the fingers in the VPL of the somatosensory thalamus (right panel of Fig. 1C). Recordings were performed contralateral to the stimulated hand (right) and ipsilateral to the responding hand (left). Each recording began with a mapping session to find the cutaneous representation of the fingers in VPL. Subsequently, we mapped neurons in S1 sharing receptive fields with the neurons of VPL (Fig. 1D). All recorded neurons had small cutaneous receptive fields with quickly (QA, VPL n = 65, S1 n=71) or slowly adapting (SA, VPL n = 9, S1 n=4) properties. Locations of the electrode penetrations in VPL and S1 were confirmed with standard histological techniques. The neuronal signal of each microelectrode was sampled at 30 kHz and spikes were sorted online. A more extensive description of the task and recording procedure can be found in previous publications (1, 3).

Here, we report data from multiple recording sessions during which spikes were obtained. For the experimental condition, we recorded 47 sessions with 120−140 trials per session (53 neurons in VPL, 75 neurons in S1, 84 VPL-S1 pairs). For the passive control condition, we obtained 21 sessions with 70-140 trials (21 neurons in VPL, 36 neurons in S1). We performed a fully balanced comparative analysis between the original and control task recordings to mitigate confounding effects. To do so, we only considered VPL-S1 neuron pairs that were recorded in both

experimental conditions. In addition, for each of these pairs, we performed trial subsampling to obtain the same type and number of amplitude classes recorded in the vibrotactile detection and the passive stimulation task. As a result, the pairing pre-processing yielded 36 VPL-S1 pairs that were recorded in both conditions: 1307 stimulus-present trials and 1364 stimulus-absent trials that could be used for unbiased statistical comparison (Fig. 6). In the comparative analysis, we removed the first two intervals of both tasks due to the presence of signal artifacts in the passive condition. Hence, this analysis was restricted to the sub-period $0.5 - 5$s in both tasks (Fig. 6).

Single-trial *DI* estimation: Pre-processing, quantification and significance testing.

We used custom-built MATLAB codes to analyze the data. The directionality analysis presented here is a refinement of our previous method to analyze spike-train directional correlations (4). We estimated directional information between every neuron pair within a population using a Bayesian estimator of the directed information-theoretic measure (5) between a pair of discrete time series that were assumed to be generated according to a Markovian process. In more specific terms, for a pair time series (x^T, y^T) of length T, where $x^T = (x_1, \dots, x_T)$ and $y^T = (y_1, \dots, y_T)$, a time delay $D \geq 0$, and Markovian orders equal to $M_1 > 0$ and $M_2 > 0$, respectively, the directed information-theoretic measure between the underlying stationary processes of x^T and y^T, i.e., (X, Y), is estimated through the formula:

$$\hat{I}_D(X \to Y) \triangleq \frac{1}{T}\sum_{t=1}^{T}\sum_{y_t}\hat{P}\left(Y_t = y_t \middle| X_{t-D-M_2}^{t-D} = x_{t-D-M_2}^{t-D}, Y_{t-M_1}^{t-1} = y_{t-M_1}^{t-1}\right) * log\frac{\hat{P}\left(Y_t=y_t \middle| X_{t-D-M_2}^{t-D}=x_{t-D-M_2}^{t-D}, Y_{t-M_1}^{t-1}=y_{t-M_1}^{t-1}\right)}{\hat{P}\left(Y_t=y_t \middle| Y_{t-M_1}^{t-1}=y_{t-M_1}^{t-1}\right)},$$

[Eq. S1]

where, the joint and marginal probability distributions of (X, Y) are estimated using the context-tree weighting algorithm (CTW, [6, 7]). Matlab code for the CTW-based

estimation of the directed information-theoretic measure can be downloaded from https://web.stanford.edu/~tsachy/DIcode/. Equation 1 quantifies the information that the past of X^T at delay D, i.e., $X_{t-D-M_2}^{t-D}$, has about the present of Y^T, i.e., Y_t, given the most recent part of Y^T, i.e., $Y_{t-M_1}^{t-1}$. This estimator is consistent as long as the two neuronal time series (X^T, Y^T) form a jointly stationary irreducible aperiodic finite-alphabet Markov process whose order does not exceed the prescribed maximum depth in the CTW algorithm (6). Prior to estimating the directed information-theoretic measure, we preprocessed our data as follows. For a single trial, we first binarized spike-train trials using bins of 1ms (mapping 1 to each bin with at least one spike and 0, otherwise). Second, in stimulus-present trials, we removed the variable-time pre-stimulus period in every trial and aligned all trials to the stimulus onset time. In contrast, in stimulus-absent trials, we aligned the trials to the probe down event (PD). We then divided each trial time series into twenty non-overlapping task intervals of 0.25s (250 bins). At each task interval, the spike train was assumed to be generated by a random process that satisfied the estimator requirements with a maximum memory of 2ms ($M_1 = M_2 = 2$ bins) both for the joint and the marginal spike-train processes. Under the estimator requirements, it can be easily checked that the directed information-theoretic measure is asymptotically equivalent to the transfer entropy measure (8) in the limit of the time-series length. To assess that neurons were able to express minimal information through their spike-train responses, we assessed the significance of the entropy value (a particular case of the directed information-theoretic measure when X^T and Y^T coincide) of each spike train at every task interval with maximum memory, $M = 2$. This step removed segments of spike trains with zero or small number of spikes. Finally, among those pairs of spike-train segments with significant entropy, we ran the delayed directed information-theoretic measure estimator (Eq. S1) at time delays D=0, 2, 4, 6, 8, 10, 12, 14, 16, 18, 20 ms.

We dealt with the multiple test problem over delays by using the maximum directed information-theoretic measure over all preselected delays as a test statistic:

$$I_{\mathrm{STAT}}(X \to Y) \triangleq \max_{D\epsilon[0,2,\cdots,20]} \hat{I}_D\,(X \to Y) \qquad \text{[Eq. S2]}$$

To assess the significance of the above statistic (Eq. S2), we used a Monte-Carlo permutation test (9). In this test, the original (i.e., non-permuted) estimation was compared with the tail of a distribution obtained by performing 20 equally-spaced (to maximize independent sampling) circular shifts of the target spike train Y^T within the range [50,200]ms and computed the corresponding P-value (10). Hence, the significance test provides three outputs: the significance assessment $(0/1)$, the statistic value and the maximizing delay $\widehat{D}$. In particular, any spike-train pair during a trial is considered to convey directional information (*DI*) at a given task interval if the corresponding test yields significance.

Statistical analysis: Quantification of significant effects on *DI* percentages

The main metric used in Figs. 3-7 was obtained by aggregating each *DI* type (feedforward, feedback and bidirectional) over all neuron pairs and trials at individual task intervals and computing their percentage over the total amount of trials. In Fig. 8, however, the percentage was computed over trials per neuron pair and then percentages were averaged over neuron pairs.

Therefore, the main results illustrated in Figs. 3-8 were obtained by comparing *DI* percentages under usually two conditions. Comparisons of this metric were of two types: paired and unpaired. Paired comparisons appeared in the comparison between the VPL→S1 and VPL→S1 percentages (Fig. S1), the percentages over neuron pairs in different conditions (Fig. S3), the percentages between the original and control task (Fig. 6) and the percentages over neuron pairs for correct and error trials (Fig. 8). Unpaired comparisons appeared when assessing the stimulus-driven change in the percentage of directional information (Figs. 3A, 7A). In paired or unpaired comparisons of *DI* percentages we frequently used non-parametric tests for correlated samples (11) using statistics based on Cohen's effect size (Cohen's *h*; [12]) that measured the distance between proportions. The use of this statistic allows to straightforwardly quantify the size of any significant effect by comparing

its value with standarized thresholds (*H = 0.2*, small effect size; *H = 0.5*, medium effect size; *H = 0.8* large effect size), thus avoiding sample size biases. For any unpaired comparison between proportion p_1 and p_2, we used the original Cohen's *h* measure:

$$H^{\text{unpaired}}(p_1, p_2) = 2\left(\arcsin\sqrt{p_1} - \arcsin\sqrt{p_2}\right) \quad \text{[Eq. S3]}$$

For paired comparison, we proposed the following paired version of Cohen' *h*:

$$H^{\text{paired}}(p_1, p_2) = \text{sign}(\bar{p}) * 2\arcsin\sqrt{|\bar{p}|} \quad \text{[Eq. S4]}$$

where $\bar{p} = \frac{p_1 - p_2}{2}$.

Non-parametric tests for correlated samples were performed through 1000 group-based permutations (11) where groups were defined to be either single trials (Figs. 3-7) or neuron pairs (Fig. 8) and group sample sizes were maintained in each permutation. Thus, our analysis avoided introducing any statistical bias to the sampled reference distribution. Most statistical comparisons were independently performed over task intervals (*N = 20*). To correct for interval multiplicity (e.g. Fig. S1), we applied the Holm-Bonferroni procedure (13), which provided a significance threshold that controlled the Familywise Error Rate (FWER) at a significance level (α *= 0.05*). In the remaining tests performed at different amplitude values or neuron pairs, multiplicity was not corrected for lack of sufficiently large sample sizes.

In Fig. 6B we applied single-trial and average-trial correlation measures to quantify the non-parametric correlation (Spearman's rank-order correlation) between *DI* percentages and stimulus amplitudes. Single-trial correlation values were obtained by correlating the trial-based binary vector associated to each *DI* type against their corresponding amplitudes. Average-trial correlations were obtained by first computing the overall percentage of *DI* at each amplitude and then by correlating these percentages against all amplitude values.

Statistical analysis: Influence of neuronal firing rates into *DI* percentages

A great deal of the results was devoted to assess the influence of the firing rates of driver and target neurons into the *DI* measured in our data set (Figs. S4, S7A and B, 4 and 7). In particular, we made of use of Spearman's correlation to correlate the firing rate of simultaneous neuronal spike trains in VPL and S1 with the existence of *DI* $(0/1)$ between them across all trials. More precisely, we independently correlated the trial-based binary vector associated to the *DI* against the firing rate in VPL and S1 spike trains, respectively. We performed this computation in general for the *DI* against driver and target firing rates (Figs. S4A and S4B), and in particular for each *DI* type, feedforward, feedback and bidirectional, against VPL and S1 firing rates in every task interval (Figs. S4C and S4D and Figs. S7A and S7B). Moreover, we compared the firing rates of neurons in VPL and S1 holding the distinct *DI* types (Figs. 4, 7B and C). These later comparisons are intrinsically unpaired (in trials) as the amount of *DI* trials may differ across types. Hence, we made use of Wilcoxon rank-sum test to assess statistical differences in *DI*-dependent firing rates.

Statistical analysis: Contribution of zero-lag and non-zero lag to bidirectional information

By definition (See section "Single-trial *DI* estimation" above), each *DI* is associated to a (maximizing) delay. Hence, to study the contribution of individual time delays to each *DI* type we started by plotting their histograms in Fig. S2B using aggregated data from task intervals within or outside the stimulus period and the PWS. These histograms pinpointed the great percentage of bidirectional information at time delay 0 ms, especially during the stimulus-presence. We therefore examined in Fig. 7 and S7 the contribution of 0 ms delays to the main results reported for bidirectional information. To do so, we divided all bidirectional information estimates into two disjoint groups: one bidirectional group where the *DI* across each direction was estimated at 0 ms delay, and a second group where both were estimated at a delay different from 0 ms. The formed group is referred

in the main text as zero-lag bidirectional information, whereas the second group is referred to as non-zero lag bidirectional information. We then considered these groups as *DI* sub-types and performed on them the main analysis of the study in Fig. 7 and Fig. S7. Specifically, we repeated those analyses leading to Fig. 3A (Fig. 7A), Fig. 4 (Fig. 7B and 7C), Fig. S4 (Fig. S7A and S7B), Fig. 5 (Fig. S7C) and Fig. 6 (Fig. 7D).

Simulation study

In Fig. S5, we made use of two stochastic models (Unidirectional and Bidirectional) to simulate pairs of spike trains from two different neurons eliciting firing rates within the range of our dataset and assess the sensitivity of our *DI* estimation method and the correlation between the *DI* and the firing rate induced by the estimation method. The simulation of spike-train pairs was randomly and independently generated on a trial-by-trial basis according to two paradigms: a unidirectional model, which is associated to the reported feedforward and feedback information, and a bidirectional model, which is associated to bidirectional information. Under each paradigm, single-trial spike trains were modeled as binary sequences generated via conditional probabilities relying on *signal* (δ, λ) and *noise* parameters (ε, ν). The range of these parameters was chosen to fit the range of neuronal firing rates found during the first half (250ms) of the stimulus period during hit trials. Each model was used to test the sensitivity of the *DI* estimation against the firing rate of either the target, driver or both simultaneous recorded neurons (Fig. S5C and S5D). In particular, we used the bidirectional model to test whether the *DI* sensitivity was significantly different between zero-lag and non-zero lag bidirectional information. In addition, each model served to test the correlation of the *DI* with the firing rate. To obtain a fair comparison with the correlation values observed in the real data, each model was mixed with realizations of independent spike train pairs so that the simulated data mimicked the overall *DI* percentage observables while still approximating the average firing rates in driver and target neurons (Fig. S5E and S5F). Then, the correlation values were shown as a function of increasing *DI* percentages (Fig. S5G and S5H), which corresponded to increasing weights of each paradigm in the mixed model. Further details can be found in Fig. S5.

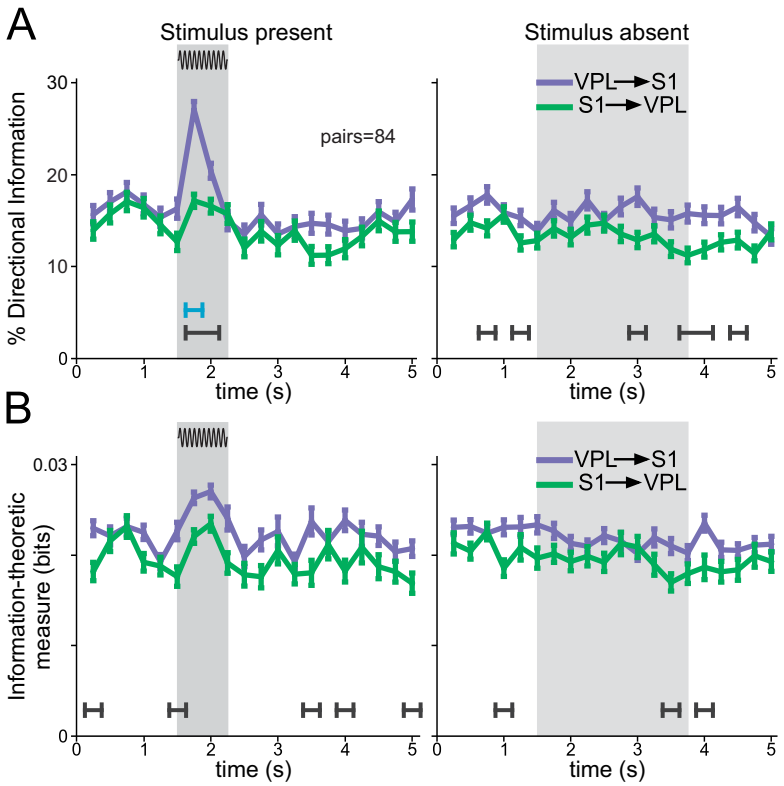

Fig. S1. VPL→S1 and S1→VPL directional information (*DI*) during the detection task. Time course of the task for the percentage of directional information (*DI*) and the average (unbiased) information-theoretic measure estimate over *DI* pairs between VPL→S1 (purple) and S1→VPL (green) in stimulus-present (left panel, trials = 3216 hit; neuron pairs = 84) and stimulus-absent trials (right panel, trials = 4371 correct rejections; neuron pairs = 84). Only paired trials where at least one spike train attained a minimal firing rate of 35Hz were selected for the computation. In all figures, grey boxes depict the stimulation period for the stimulus-present trials, and the possible window of stimulation (PWS) for the stimulus-absent trials). Error bars denote the SEM (standard error of the mean). (A) Percentage of *DI*. Black lines depict intervals for which the difference between *DI* was significantly different ($P < 0.05$; non-parametric test, multiple-test corrected; effect size > 0.3). Blue lines depict significant intervals for which the effect size was larger than 0.5. (B) Time course of information-theoretic measure for VPL→ S1 (purple) and S1→ VPL (green) directional information. Black lines depict intervals for which the difference between directions was significantly different ($P < 0.05$; non-parametric test, multiple-test corrected; effect size > 0.3). Here and in the next time-varying figures, we removed the variable-time pre-stimulus period in every stimulus-present trial and aligned all trials to the stimulus onset. In stimulus-absent trials, we aligned the trials to the probe down event (PD).

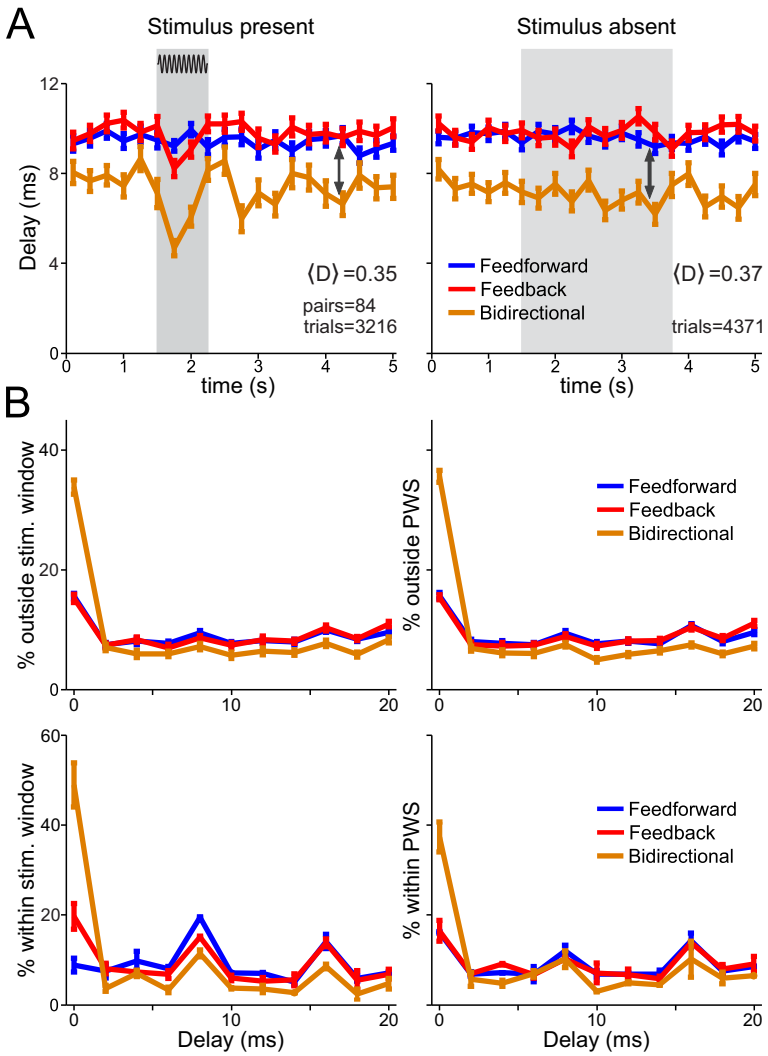

Fig. S2. Mean delay for feedforward, feedback and bidirectional information. Related to Fig. 3 (A) Time course of the task for the mean delays occurring during feedforward, feedback and bidirectional information for stimulus present (left, trials=3216 hits; neuron pairs = 84) and stimulus absent (right, trials=4371 correct rejections; neuron pairs = 84) trials. ⟨D⟩ Indicates the average value of the Cohen's D effect size (over task intervals and *DI t*ypes) between joint feedforward and feedback, and bidirectional information. (B) Percentage of delays outside (upper panel) or within (lower panel) the stimulation or possible window of stimulation (PWS) for stimulus present (left) and stimulus absent (right) trials, respectively. Error bars denote the SEM (standard error of the mean).

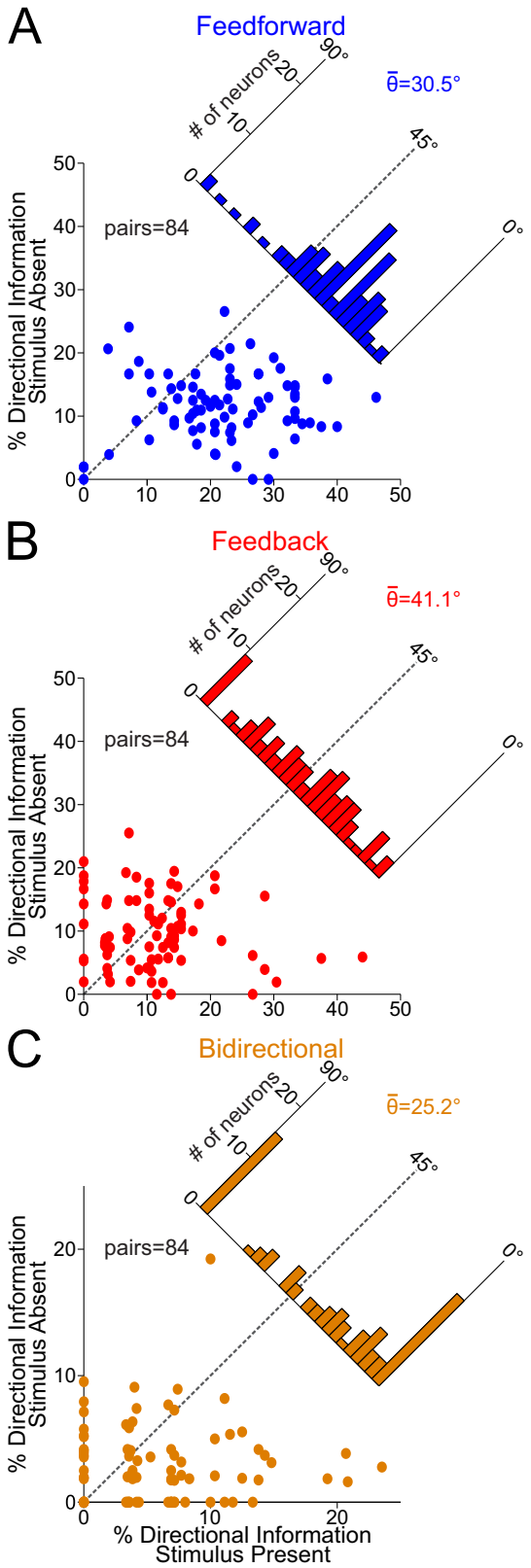

Fig. S3. Directional Information (*DI*) comparison between stimulus-present and stimulus-absent trials. Related to Fig. 3. Percentage of (A) feedforward, (B) feedback, and (C) bidirectional information per neuron pair (trials = 3216 hits; trials = 4371 correct rejections; neuron pairs = 84) during the first interval (0-0.25s) of the stimulus period in stimulus-present trials vs. the first interval (0-0.25s) of the possible window of stimulation (PWS) in stimulus-absent trials. In each panel the insets depict the histograms of the angular deviation between stimulus-absent and stimulus-present trials over all neuronal pairs and indicates its median. The percentage for all three types of *DI* was higher during the stimulus-present trials ($\theta < 45°$) with feedforward ($\theta = 30.5°$) and bidirectional ($\theta = 25.2°$) information exhibiting larger differences across conditions than feedback ($\theta = 41.1°$) information.

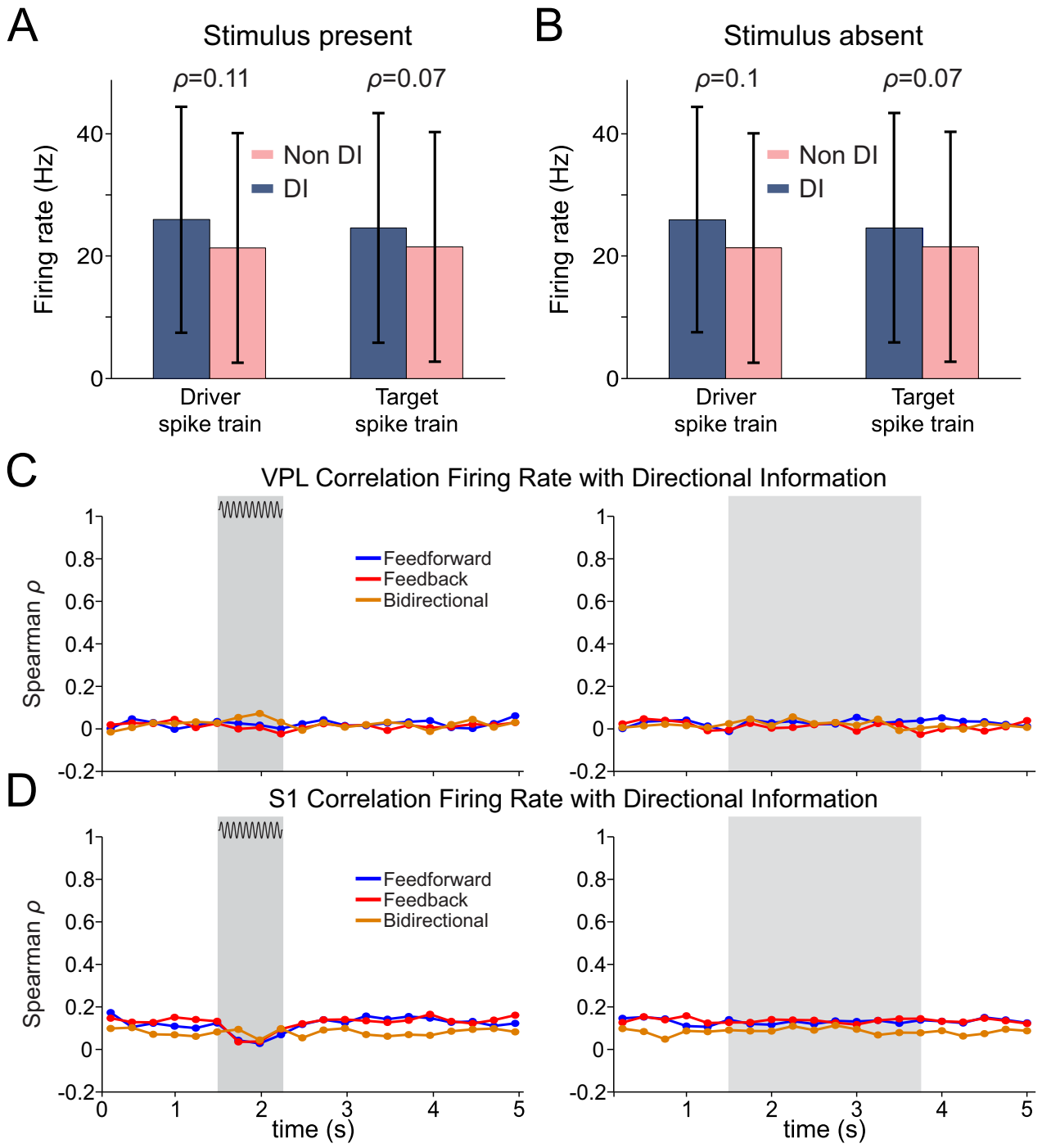

Fig. S4. Correlation between firing rate and directional information (*DI*) types. Related to Fig. 3 and 4. Mean firing rate for driver and target neurons holding *DI* and non *DI* across the VPL→S1 and S1→VPL neuron pairs (84). (A) Mean firing rate and standard deviation for driver and target neurons for the stimulus-present trials. Blue depicts firing rates related to *DI* (*DI* intervals = 29074; trials = 3216 hits). Pink depicts firing rates related to non *DI* (non-*DI* intervals = 177286). The value of ρ indicates the Spearman correlation value obtained from correlating the firing rate of the driver/target with the existence of incoming/outgoing *DI*. (B) Same as in (A) but for the stimulus-absent trials (*DI* intervals = 28253; non-*DI* intervals = 178027; trials = 4371 correct rejections). (C) Spearman's correlation between the firing rate in VPL neurons and the existence of feedforward, feedback or bidirectional information with a S1 neuron during the time course of the task during stimulus-present (left; trials = 3216 hits) and stimulus-absent (right; trials = 4371 correct rejections) trials. (D) Similar as panel C, but for S1 neurons holding *DI* with VPL neurons.

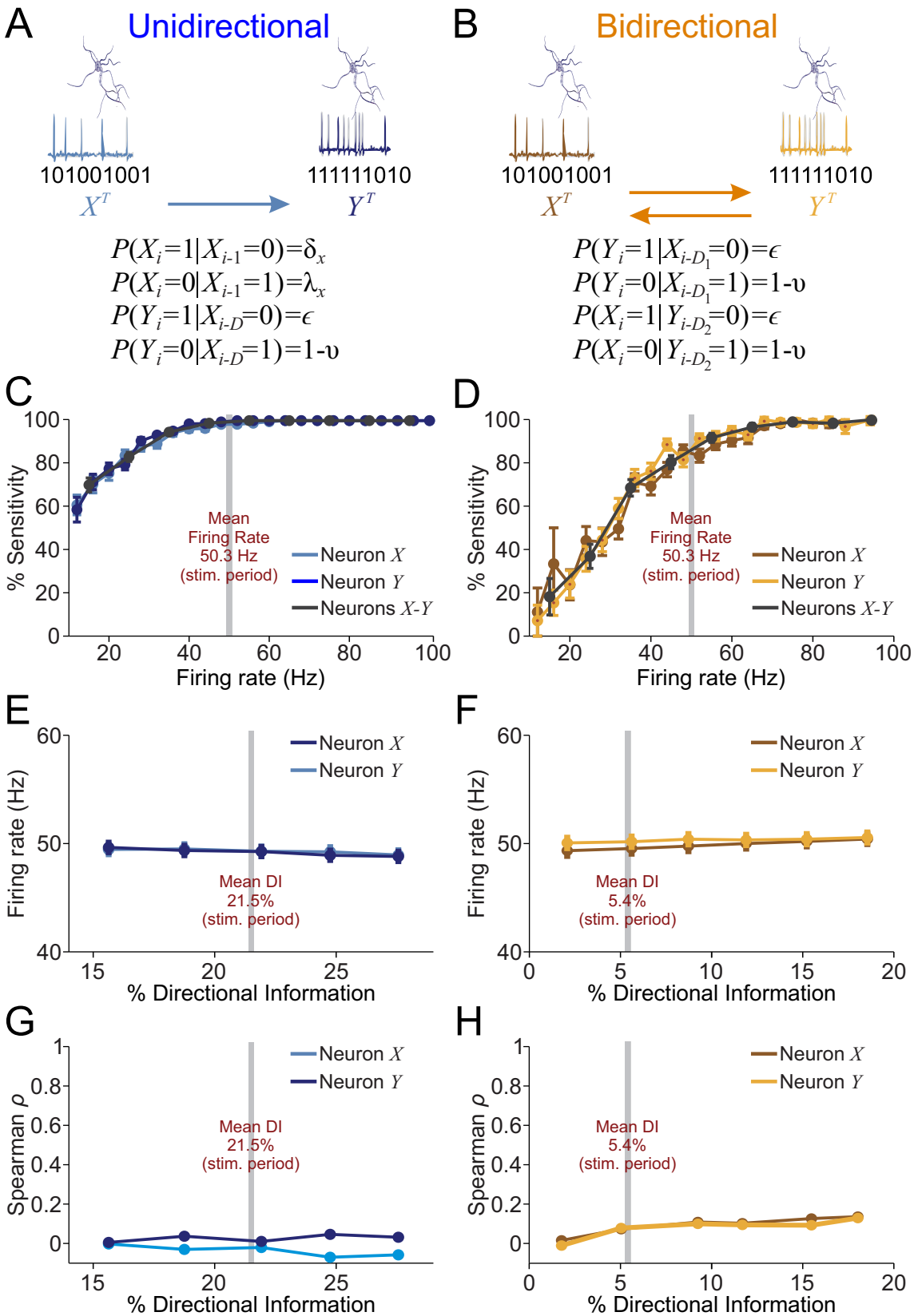

Fig. S5. Unidirectional and Bidirectional simulation models. Related to Fig. 3 and 4. We simulated pairs of spike trains (N=3850 trials) from two different neurons eliciting firing rates within the range of our data set to assess (1) the sensitivity of our *DI* estimation method and (2) the correlation between the *DI* and the firing rate induced by the estimation method. Pairs of spike trains were randomly and independently generated according to two simulation paradigms: unidirectional model, which is associated to the reported feedforward and feedback information, and bidirectional model, which is associated to bidirectional information. Under each paradigm, single-trial spike trains were modeled as T-length binary sequences ($X_T=[X_1,...,X_T]$ and $Y_T=[Y_1,...,Y_T]$), which were generated by probabilistic models with parameters chosen to fit the range of neuronal firing rates found during the first half (250ms) of the stimulus period during hit trials. (A) Unidirectional model: The single-trial spike train of the driver neuron is denoted as X^T and is modeled as a binary Markov chain of order 1 with two autocorrelation parameters (δ_x, λ_x), which characterize the *neuronal*

signal, i.e., the spiking probability of X^T after a silent bin, $\delta_X = P(X_i=1 | X_{i-1}=0)$ and the spiking probability of X_T after a spike, $\lambda_X = P(X_i=1 | X_{i-1}=1)$. On the other hand, the single-trial spike train of the target neuron is denoted as Y^T and is characterized by a transformation of the process X^T that depends on 3 parameters (D, ε, v). D stands for the delay at which the coupling between both spike trains occurs while ε and v parametrize the *channel noise*, i.e., the spiking probability of Y^T after a silent bin, $\varepsilon = P(Y_i=1 | X_{i-D}=0)$, and the spiking probability of Y^T after a spike bin in X^T, $v = P(Y_i=1 | X_{i-D}=1)$. (B) Bidirectional model. The bidirectional coupling between X^T and Y^T is modeled by 4 parameters (D_1, D_2, ε, v). D_1 and D_2 stand for the delays in each direction at which the coupling occurs, respectively, while ε and v parametrize in an unbiased form the noise across both unidirectional links, $X_T \rightarrow Y_T$ and $Y_T \rightarrow X_T$. (C)-(D) Sensitivity percentage of the *DI* estimation for both simulation models. Gray line in each panel depicts the mean neuronal firing rate in real-data recordings during the first half of the stimulus period during hit trials (50,33Hz). Curves that are function of joint target and driver neurons are constructed by binning firing rates from both neurons in consecutive 10Hz bins (10-20Hz, 20-30Hz, etc.) and plotting the sensitivity values at bin midpoints. Error bars denote the SEM (standard error of the mean) across simulation realizations. (C) Sensitivity percentage of the *DI* estimation method in the unidirectional model as a function of firing rate of the driver (X^T), target (Y^T) and both neurons. In total, an ensemble of spike train pairs (simulated trials=3850) were uniformly generated with T=250 bins across autocorrelation parameters δ_X=0.02:0.01:0.08 and λ_X=0.05, and noise parameters ε=0.013 and v=0.35:0.1:0.45. Delays were uniformly drawn over D=0:2:20 bins. Error bars denote the SEM (standard error of the mean). (D) Sensitivity percentage of the *DI* estimation method in the bidirectional model as a function of firing rate of the driver (X^T), target (Y^T) and both neurons. In total, spike train pairs (simulated trials=1925) were uniformly generated with T=250 bins across noise parameters ε=0.013 and v=0.35:0.1:0.45 and delays uniformly drawn over D_1, D_2 =0:2:20 bins. Error bars denote the SEM (standard error of the mean). In this model the difference between the sensitivity of zero-lag and non-zero lag bidirectional information was not found significant (Wilcoxon rank-sum test, P>0.05, SI Appendix). (E)-(H) To fit the *DI* estimation percentages found in real data recordings, both models were mixed with an ensemble of independently generated spike train pairs (simulated trials =3850 for unidirectional model; simulated trials =1925 for bidirectional model) with autocorrelation parameters δ_X=0.02:0.01:0.08 and λ_X=0.05. To sample different *DI* percentages, the mixing factor α varied from α=0 (all pairs belong to the independent ensemble) to α=1 (all pairs belong to the uni/bidirectional model) in steps of 0.04 keeping always the total number of trials equal. In each panel, the gray line depicts the overall *DI* percentage for either unidirectional (21.5%) or bidirectional information (5.4%). Error bars denote the SEM (standard error of the mean) across simulation realizations. (E) Average firing rate of driver (X^T) and target neurons (Y^T) in the mixed unidirectional model as a function of the *DI* percentage. (F) Same as Panel (E) but for the mixed bidirectional model. (G) Correlation between *DI* and the driver (X^T) and target neurons (Y^T) firing rate in the mixed unidirectional model as a function of the *DI* percentage. (H) Same as panel E, but for the mixed bidirectional model.

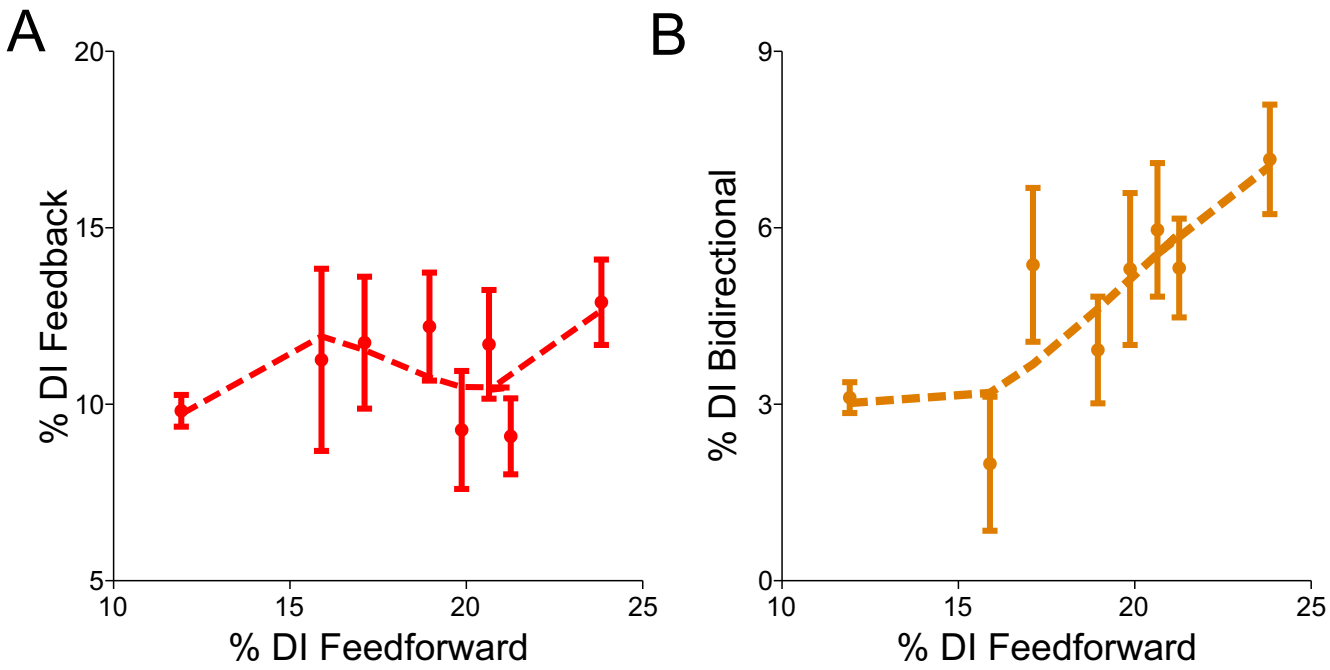

Fig. S6. Relationship of the amount of feedback and bidirectional information with respect to feedforward information across distinct stimulus amplitudes. Related to Fig. 5 (A) Relationship between %*DI* feedback and %*DI* feedforward for all stimulus amplitude values analyzed in the study. (B) Relationship between %*DI* bidirectional and %*DI* feedforward for all stimulus amplitude values analyzed in the study. Error bars denote the standard error of the mean (SEM).

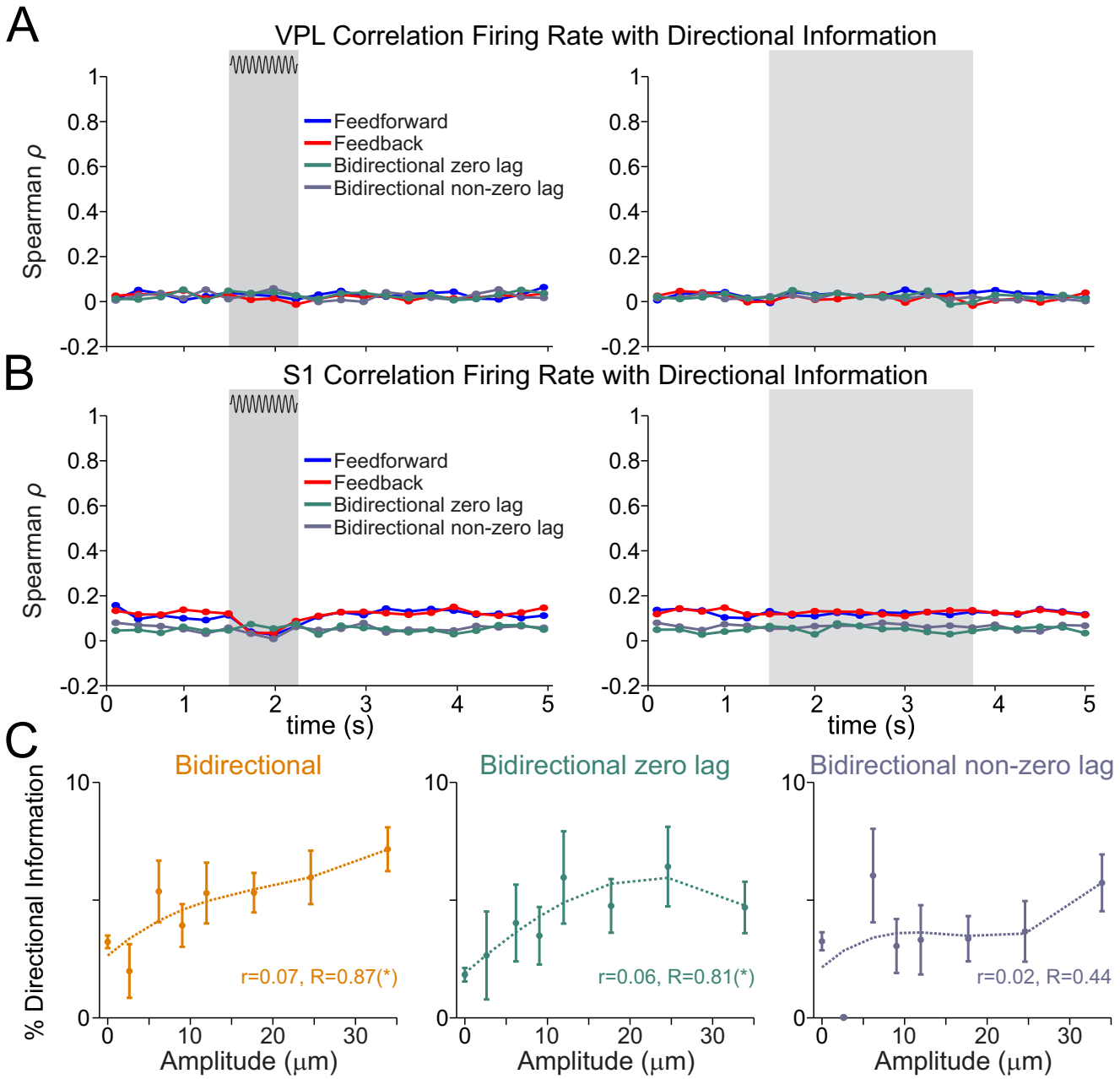

Fig. S7. Influence of neuronal firing rate and stimulus amplitudes on zero-lag and non-zero lag bidirectional information. Related to Fig. 8 (A) Spearman's correlation between the firing rate in VPL neurons and the existence of overall and either zero-lag or non-zero lag bidirectional information, respectively, with a S1 neuron during the time course of the task during stimulus-present (left; trials = 3216 hits) and stimulus-absent (right; trials = 4371 correct rejections (B) Same as panel A, but for neurons in S1 holding bidirectional information with VPL neurons. (C) Mean percentage of overall (left), zero-lag (middle) and non-zero lag (right) bidirectional information as a function of the stimulus amplitude during the first half of the stimulation period (left, 0 − 0.25 s). The value of *r* is the correlation between the stimulus amplitude and the existence of *DI* in each type across all trials (no amplitude-averages) with Spearman correlation (trials = 7587). The value R is the analogous correlation considering amplitude-average values (amplitudes = 8). Asterisks depict significance (*, $P < 0.05$; Spearman correlation). Error bars denote the SEM (standard error of the mean).

References

1. Vázquez, Y., Zainos, A., Alvarez, M., Salinas, E., and Romo, R. (2012). Neural coding and perceptual detection in the primate somatosensory thalamus. Proc. Natl. Acad. Sci. USA *109*, 15006–15011.

2. Romo, R., Brody, C.D., Hernández, A., and Lemus, L. (1999). Neuronal correlates of parametric working memory in the prefrontal cortex. Nature *399*, 470–473.

3. Hernández, A., Nácher, V., Luna, R., Alvarez, M., Zainos, A., Cordero, S., Camarillo, L., Vázquez, Y., Lemus, L., and Romo, R. (2008). Procedure for recording the simultaneous activity of single neurons distributed across cortical areas during sensory discrimination. Proc. Natl. Acad. Sci. USA *105*, 16785-90.

4. Tauste Campo, A., Martinez-Garcia, M., Nácher, V., Luna, R., Romo, R., and Deco, G. (2015). Task-driven intra- and interarea communications in primate cerebral cortex. Proc. Natl. Acad. Sci. USA *112*, 4761–4766.

5. Massey, J. (1990). Causality, feedback and directed information. In Proc. Int. Symp. Inf. Theory Applic. 27–30.

6. Jiao, J., Permuter, H.H., Zhao, L., Kim, Y.H., and Weissman, T. (2013). Universal estimation of directed information. In IEEE Trans. on Inform. Theory 59, 6220–6242.

7. Willems, F.M., Shtarkov, Y.M., and Tjalkens, T.J. (1995). The context-tree weighting method: basic properties. IEEE Trans. Inf. Theory 41, 653-664.

8. Schreiber, T. (2000). Measuring Information Transfer. Phys. Rev. Lett. *85*, 461-464.

9. Ernst, M.D. (2004). Permutation Methods: A Basis for Exact Inference. Stat. Sci. *19*, 676–685.

10. Phipson B., and Smyth G.K. (2010). Permutation P-values should never be zero: calculating exact P-values when permutations are randomly drawn. Stat Appl Genet Mol Biol, 9.

11. Winkler, A.M., Ridgway, G.R., Webster, M.A., Smith, S.M., Nichols, T.E. (2014). Permutation inference for the general linear model. Neuroimage *92*, 381-397.

12. Cohen, J. (1988). Statistical power analysis for the behavioral sciences. Stat. Power Anal. Behav. Sci. *2*, 567.

13. Holm, S. (1979). A Simple Sequentially Rejective Multiple Test Procedure. Scand J Stat. *6*, 65–70.